Eleventh International Conference on CFD in the Minerals and Process Industries
CSIRO, Melbourne, Australia
7-9 December 2015

APPLICATION OF PROPER ORTHOGONAL DECOMPOSITION (POD) TECHNIQUES AND SCALE-RESOLVING CFD SIMULATIONS TO STUDY SWIRLING FLOW IN AN AXISYMMETRIC SUDDEN EXPANSION

Clint HOWARD, Ali ABBAS, Timothy A.G. LANGRISH and David F. FLETCHER*

[1] School of Chemical and Biomolecular Engineering, The University of Sydney, NSW 2006, AUSTRALIA
*Corresponding author, E-mail address: david.fletcher@sydney.edu.au

ABSTRACT

CFD simulations of swirling flow in an axisymmetric sudden pipe expansion are performed and used to understand the structure of the flow. The *k*-ε and SAS model coupled with zonal LES available in ANSYS CFX 15 is used to model turbulence. As well as conventional analysis using typical CFD post-processing techniques and Fast Fourier Transforms (FFTs), Proper Orthogonal Decomposition (POD) is used to extract reduced order models of the wall pressure data. The ultimate aim of this work is the development of control strategies to reduce wall deposition in particle-laden flows.

NOMENCLATURE

d	inlet pipe diameter
D	large pipe diameter
f	frequency
k	turbulence kinetic energy
p	pressure
r	radial coordinate
Re	Reynolds number (defined in eqn. (1))
S	swirl number (defined in eqn. (2))
St	Strouhal number (= $4fD/\pi u_{in}$)
u	fluid velocity
ε	turbulence energy dissipation rate
λ	objective function (defined in eqn. (4)
μ	dynamic viscosity
ρ	fluid density
ω	fluid angular velocity at inlet

subscripts

a	axial
in	inlet
t	tangential

INTRODUCTION

Swirling flow in an axisymmetric sudden expansion provides an excellent geometry in which to perform experimental and computational studies of an important class of industrial flows. Swirling flows are used in spray dryers in order to stabilise the flow and to increase the mixing and residence time of the spray (Fletcher et al., 2006). They also represent a simplified model of various combustion devices used to power aircraft or to generate power (Wegner et al., 2007).

Although a sudden pipe expansion is a very simple geometry, if swirl is introduced the flow is found to exhibit very complicated behaviour. The pioneering experimental work of Dellenback et al. (1988), in which the effect of changing the inlet swirl and Reynolds number using a 2:1 axisymmetric sudden expansion was investigated has often been used as a test case in this area. The key observation was that as the swirl number was increased the flow changed from steady at zero inlet swirl, to showing a weakly precessing central vortex in the opposite sense to the imposed swirl until a swirl number of approximately 0.15 was reached (depending on the Reynolds number) and then strong precession in the same sense as the imposed swirl for increasing swirl numbers. Vortex breakdown occurred at swirl numbers in the region of 0.35-0.4, leading to strong reverse flow on the axis.

These experiments were modelled using the CFX4 code by Bao, Langrish and Fletcher (2001) using the *k*-ε turbulence model on a structured mesh having 200,000 cells. This model was able to reproduce the main features of the flow, including the precession behaviour and the variation of the Strouhal number with inlet swirl. However, due to limitations of computing resources at the time and the state of development of turbulence models these simulations were necessarily limited in the detail they could capture.

Since then much work has been done to investigate the performance of Reynolds-averaged turbulence models for unsteady flows. Menter and Egorov (2010) showed that when run in transient mode the *k*-ε produces mono-frequency unsteady features, with the scale being determined by a characteristic dimension of the system rather than that of the true underlying flow structure. Modification of the model to introduce an extra term, which includes the von Karman length-scale, allows the scale to adjust to the underlying mesh and capture the turbulence structures on as fine a scale as the mesh allows. This model is called the Scale Adaptive Simulation (SAS) model. Egorov et al. (2010) have demonstrated the applicability of this model to a wide range of flows and it has now been validated extensively.

Fletcher and Langrish (2009) applied the model to a pilot scale spray dryer and demonstrated that the SAS model gave much more physically realistic results for the flow in the dryer. Specifically, the oscillatory frequency of the jet was more complex and small-scale flow structures were present throughout the dryer, producing a flow field that was much more consistent with that observed experimentally than that from a *k*-ε model.

This paper has a number of objectives in a bid to better understand such flows and their structure. These are as follows:

- Revisit the 2:1 expansion flow and apply the latest turbulence models and numerical methods to see how they perform;
- Explicitly show how simulations using the scale resolving approach compare with those that use

Unsteady Reynolds Averaged Navier-Stokes (URANS) simulations;

- Investigate different ways to analyse the data obtained from the simulations. A key focus is to use Proper Orthogonal Decomposition (POD) techniques to extract low order models and provide insights into the flow structure.
- Provide numerical data that can be compared with results from a parallel experimental study.
- Aid with the design of active control systems to mitigate flow instabilities and prevent, for example, deposition of droplets of partially-dried products on spray dryer walls.

MODEL PROBLEM

The system considered is designed to replicate that of Dellenback et al. (1988). A 0.5 m diameter inlet pipe of length 2.5 m expands suddenly into a pipe of diameter 0.98 m (giving the 1.96 expansion ratio used in their original work) and length 10 m. This flow is characterised by two dimensionless groups, the inlet Reynolds number (Re) and the inlet swirl number (S), which are defined via

$$\mathrm{Re} = u_{in} d\rho / \mu \tag{1}$$

and

$$S = \frac{1}{r_{in}} \frac{\int u_a u_t r \mathrm{d}A}{\int u_a^2 \mathrm{d}A} \tag{2}$$

In the experiments of Dellenback et al. swirl was generated using tangential inlets. In these simulations the swirl was generated by setting a forced vortex profile at the inlet. For this assumption the swirl number is given by

$$S_{in} = \omega d / 4u_{in} \tag{3}$$

where ω is the angular velocity at the inlet.

CFD MODEL

Turbulence Models

Two different turbulence models were applied in order to investigate their impact on the computed flow solution:

1. The standard k-ε model available in ANSYS CFX 15 was applied so that the results could be compared with those found in our earlier work.
2. The SAS model, as coded in ANSYS CFX 15 was also used. Initial simulations showed that the instability in the flow is too weak to trip the SAS model into scale resolving mode at low swirl numbers, so it was combined with a zonal LES model. The LES zone extended from 2d upstream of the expansion to 6D downstream of it, so that an unsteady flow was always produced. In the LES zone a source term is applied to the k equation so that the calculated eddy viscosity is that of a Smagorinsky subgrid closure. ANSYS CFX uses a harmonic flow generator to convert modelled turbulence to resolved turbulence at the start of the LES zone. Further details of the model are available in Menter et al. (2009). The model automatically defaults to using Wall Modelled LES (WMLES) in which the laminar sublayer is modelled not resolved.

Computational Mesh

A structured computational mesh was generated using ANSYS ICEM Hexa. Care was taken to ensure the mesh was as smooth and orthogonal as possible. A number of different meshes were explored with the final mesh used being a compromise between excessive size, simulation time and good resolution. The mesh used in all the simulations presented here comprised 3.4 million nodes and is shown in Fig. 1.

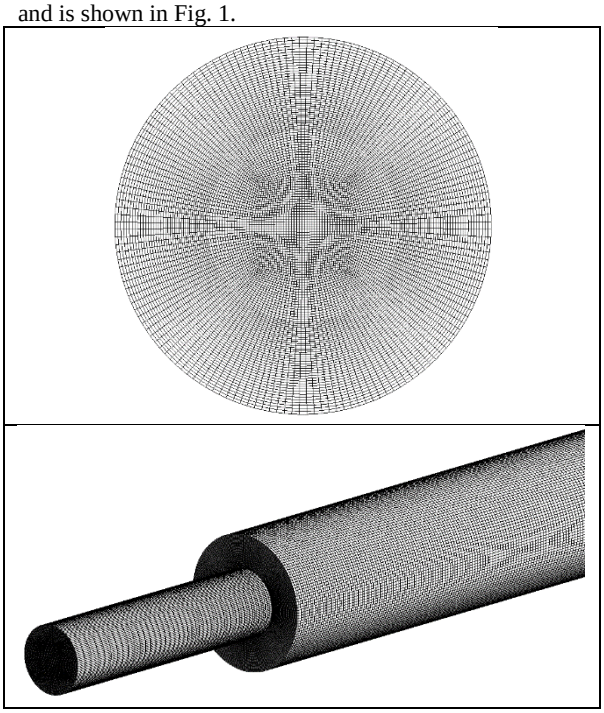

Figure 1: The computational mesh used in the simulations. The top picture shows the mesh on the inlet and wall of the expansion face. The lower picture shows the mesh distribution along the pipe.

Boundary Conditions

At the inlet a constant axial velocity and forced vortex were imposed with the values depending on the desired conditions calculated using equations (1)-(3). A no-slip boundary condition was applied at the wall together with log-law boundary conditions. At the exit an average static pressure of 0 Pa was set.

Numerical Method

The equations were solved using the vertex-centred coupled solver technology embedded in ANSYS CFX. The bounded central differencing scheme was used for the momentum equation spatial derivatives and the second order backward Euler scheme was used for the transient terms. Upwind differencing was used for the turbulence equations as recommended. At each timestep typically 3 coefficient loops were performed to ensure that the residuals of all equations fell below a normalised value of 10^{-4}. A timestep of 1 ms was used, based on the need to keep the Courant number below unity for scale-resolving simulations.

For each calculation a steady simulation using the SST model was first run to provide an initial guess. Then the transient simulation was started using the SAS model with embedded LES enabled and was run for a time of typically 20 s with the data being discarded before transient data were collected, typically then simulations were run for a period of around 100 s.

CFD RESULTS

Numerical and Modelling Aspects

When performing scale-resolving simulations it is especially important to check that the simulations have been properly implemented. The y^+ values were examined and typically they ranged from 60-80 in the inlet pipe and 10-20 in the downstream pipe. These fit well inside the acceptable range as the turbulence model is not required to predict flow separation, as this is inevitable at the expansion.

The Courant numbers were on average much smaller than unity with peak values of at most 3; with the highest values located at some intense eddies. A typical plot of the Courant number on the centre-plane for a case for Re = 10^5 and S = 0.15 is given in Fig. 2 below.

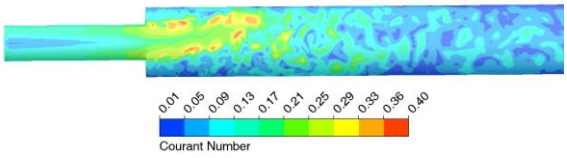

Figure 2: Courant number distribution for a case with Re = 10^5 and S = 0.15.

The turbulence model blends continuously from scale-resolving to a RANS treatment as the blending function increases from 0 to 1. It is evident in Fig. 3 below that the model is acting in SAS mode except in a thin boundary layer region around the wall.

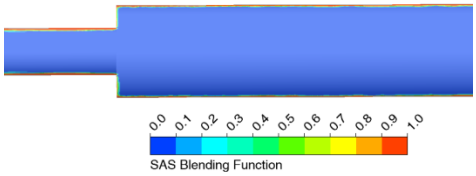

Figure 3: SAS blending function for a case with Re = 10^5 and S = 0.15.

The Q criterion, which is the vorticity squared minus the shear strain rate squared, is often used to visualise the resolved turbulence structures. Figure 4 shows a plot for a case for Re = 10^5 and S = 0.15. It is evident that there is good resolution of the turbulence structures. The start of these structures in the inlet pipe corresponds to the start of the region of the embedded LES and the structures appear developed before the inlet is reached. Towards the exit they decay not only because of natural breakdown but also because the grid is somewhat coarser so that the exit flow is less complex.

The resolved and modelled turbulence kinetic energies are shown in Fig. 5. It is evident that the turbulence kinetic energy is largely resolved, with most unresolved k being located at the walls of the inlet pipe and the shear layer immediately downstream of it. The resolved k also shows a symmetric distribution confirming that the flow has been averaged over a sufficiently long time.

Finally, a logarithmic plot of the eddy viscosity divided by the laminar viscosity is given in Fig. 6. This shows that the value is in the region of 10-40 over most of the volume, providing sufficient damping to remove the high frequency components of the turbulence, as the subgrid scale model is required to do.

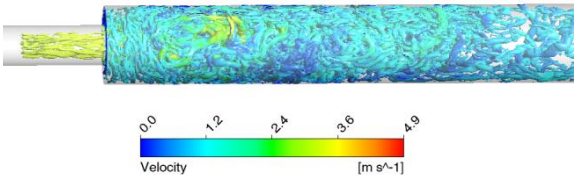

Figure 4: Isosurface of Q criterion of 100 s^{-2} coloured by velocity for a case with a Re =10^5 and S = 0.15.

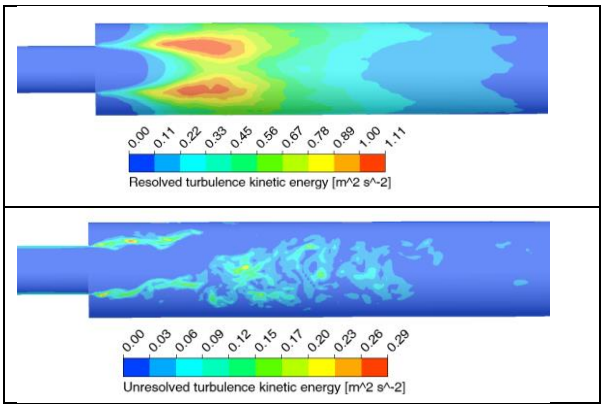

Figure 5: Plots showing the resolved (top) and unresolved (bottom) turbulence kinetic energy distributions for Re = 10^5 and S = 0.15.

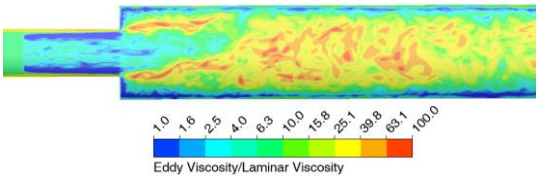

Figure 6: Plot of the normalised eddy viscosity for Re = 10^5 and S = 0.15.

Results from the k-ε model

Some simulations were run using the k-ε model in order to compare the predictions with those from a scale-resolving simulation. A Q criterion plot was created for a case with Re = 10^5 and S = 0.2 and is given in Fig. 7.

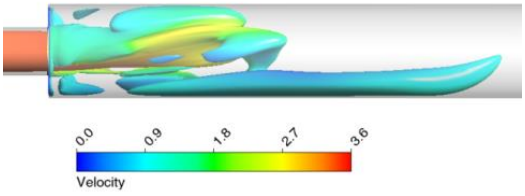

Figure 7: Isosurface of Q criterion of 10 s^{-2} coloured by velocity for a case with Re =10^5 and S = 0.2.

It is evident when Fig. 7 is compared with Fig. 4 that there are no small-scale structures and the level of vorticity is much lower as the Q criterion level plotted is 10 s^{-2} in the k-ε case, compared with a value of 100 s^{-2} in the zonal LES simulation. Plots at different times show that there are large-scale structures that precess around the axis, whereas these are much smaller and more complex in the SAS case.

FFT RESULTS

Fast Fourier Transforms (FFTs) are used to obtain information about oscillatory flows. A number of monitor points located at both the walls and along the axis of the pipe were used to record pressure and velocity data

throughout the simulations. Data were only used after a flow time of at least 40 s in this analysis so that any start-up effects were eliminated and the mean was subtracted before performing the FFT.

igure 8 shows a typical FFT plot for pressure data from a monitor located at the centre of the expansion for a low swirl case (S = 0.15, Re = 10^5). It is evident that besides the low frequency peaks there is significant power in many higher frequencies, which is typical of the type of FFT produced when using the zonal LES approach.

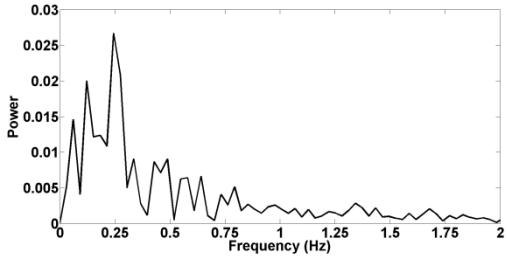

Figure 8: FFT plot for a simulation using the zonal LES model for Re = 10^5 and S = 0.15.

In contrast, for a case run using the *k-ε* model the power spectrum, Fig. 9, shows just a single peak at low frequency. It is evident that this spectrum contains very little structure which is consistent with the difference seen between Fig. 7 and Fig. 4.

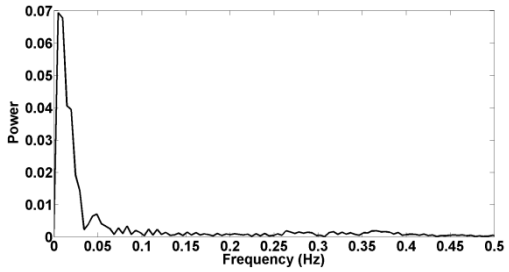

Figure 9: FFT plot for a simulation using the *k-ε* model for Re = 10^5 and S = 0.2.

Similar plots were obtained for the various swirl numbers and monitor locations analysed. The peak frequency in the S = 0.15, Re = 10^5 case gives a Strouhal number of 0.033 which is close to that of ~0.04 observed by Dellenback et al., (1988). However, detailed comparison with their work is difficult as with the current simulations there is no single peak frequency as was obtained with the *k-ε* model.

POD ANALYSIS

POD is a mathematical tool which seeks to decompose high-dimensional data into low-dimensional data whilst still retaining the key features. The decomposition provides a set of orthonormal basis functions, and it is established that these basis functions are optimal for reconstructing the original data. POD analysis effectively searches for a new mutually orthogonal coordinate system which can most effectively capture the dominant features of a system and significantly reduce the computational storage of data needed to examine the phenomena being studied (Liang et al. 2002).

POD was first introduced in the context of turbulence by Lumley (1967) and Sirovich (1987) further extended the work of Lumley by developing the method of snapshots which greatly increased the computational efficiency of the POD analysis. The classic application of POD in the field of turbulent flow involves snapshot analysis of instantaneous Particle-Image-Velocimetry (PIV) data. This application involves determining the spatio-temporal velocity flow-field and then applying POD to extract the dominant modes which highlight the coherent structures in the flow-field. This method is useful for characterising flow structures, however is of no use for flow control as it requires the use of PIV to obtain flow-data across a cross-section which is not viable in industrial applications.

Recent developments in hybrid POD methods which utilise a reduced amount of information, combined with linear stochastic estimation have led to advances in the use of POD for flow-control (Taylor (2004), Boree (2003), Bonnett et al. (1994)). This paper uses adaptations of POD from Bienkiewicz et al. (1995) and Tamura et al. (1999), who utilised it to study fluctuating pressures recorded in wind engineering applications.

Methodology

In the present study we seek to determine if pressure records at discrete points on the downstream pipe walls can be used to identify coherent structures within the pipe. The key objective of the application of the POD technique is to find a deterministic function $\Phi(x,y)$ which maximises the projection of a random pressure field $p(x,y,t)$ onto the modal function $\Phi(x,y)$, which can be considered as maximising the following normalised inner product:

$$\frac{\iint p(x,y,t)\Phi(x,y)\mathrm{d}x\mathrm{d}y}{\sqrt{\iint \Phi^2(x,y)\mathrm{d}x\mathrm{d}y}}.$$

The maximisation of the projection of the equation can be performed in the mean-square sense (since the pressure field $p(x,y,t)$ can take positive or negative values) as follows:

$$\frac{\langle \iint p(x,y,t)\Phi(x,y)\mathrm{d}x\mathrm{d}y \iint p(x',y',t)\Phi(x',y')\mathrm{d}x'\mathrm{d}y' \rangle}{\iint \Phi^2(x,y)\mathrm{d}x\mathrm{d}y}$$

$$= \lambda > 0 \qquad (4)$$

where $\langle \ldots \rangle$ denote the temporal average. The solution of this equation can be reduced to a Fredholm integral equation or eigenvalue problem.

Since here, the fluctuating pressure field is given at *M* uniformly distributed discrete time points, the Fredholm integral equation can be rewritten as a matrix equation of the form:

$$\mathbf{R}_p \Phi = \lambda \Phi \qquad (5)$$

where R_p is the auto-covariance matrix of the fluctuating pressure field $\left(\mathbf{R}_p = \mathbf{P}^T\mathbf{P}\right)$ and is an $M \times M$ square matrix. Φ and λ are the eigenvectors and eigenvalues of R_p, respectively. Solving this matrix equation yields the desired deterministic coordinate function as the eigenvectors of this equation. In theory *M* eigenvectors will be obtained and the *m-th* eigenvector Φ_m corresponds to the coordinate function $\Phi_{\mathrm{m}}(x,y)$, which in POD analysis is called the *m-th* eigenmode.

The purpose of carrying out the POD analysis lies in the extraction of the eigenmodes and the ability to use a small set of eigenfunctions as an optimal basis for the series reconstruction of the fluctuating pressure field. Using the orthogonality of the eigenfunctions, the original fluctuating pressure field is given by:

$$p(x,y,t) = \sum_{m=1}^{M} a_m(t)\Phi_m(x,y) \qquad (6)$$

where the $a_m(t)$ are the principal *m-th* coordinates or POD coefficients and can be calculated using the orthogonality of the eigenfunctions $\Phi_m(x,y)$

$$a_m(t) = \frac{\iint p(x,y,t)\Phi(x,y)\mathrm{d}x\mathrm{d}y}{\sqrt{\iint \Phi^2(x,y)\mathrm{d}x\mathrm{d}y}} \qquad (7)$$

To simplify the calculations, we can normalise the eigenvectors by setting the denominator of eqn. (7) to unity. It is noted that the POD analysis must be carried out on mean subtracted data. Including the mean value in the data will lead to a shift in the principal coordinates and this requires careful attention in the final analysis. The data presented in this paper utilise a mean-subtracted POD analysis.

The construction of the POD modes is based on the modal eigenvectors as previously discussed (Meyer et al., 2007). This reconstruction is given by:

$$\Phi_i = \frac{\sum_{m=1}^{M} A_m^i p^m}{\left\|\sum_{m=1}^{M} A_m^i p^m\right\|} \qquad (8)$$

where A_m^i is the corresponding eigenvector and p^m is the corresponding set of input vectors.

The above description outlines the methodology used in the POD analysis. However, the advantage of using it lies in the ability to use a reduced set of data to represent the original set of fluctuating pressure points. Equation (6) presents the reconstruction of the entire pressure field, and will in fact produce the original data almost identically. Reconstruction using a lower number of modes was carried out in this paper. Reconstruction using a low number of *N* modes with $N < M$ is possible, and has been shown to be quite accurate in the engineering sense to extract useful information on flow structures and pressure traces.

The number of modes needed in the reconstruction can be given by an estimate of the "energy" captured by individual modes. This "energy" relates to the dominance of each individual mode, and POD analysis is set up so that this is characterised by the value of λ_i. The proportional "energy" of each λ_i is defined as

$$e_m = \frac{\lambda_m}{\sum_{m=1}^{M} \lambda_m} \qquad (9)$$

It is then possible to estimate the "energy" captured by *N* eigenmodes by summing e_m for the chosen number of modes. In essence, the first 3-5 eigenmodes are often enough to capture over 90-95% of the energy of the system, as is shown later.

The POD tool was developed using MATLAB R2014a and the snapshot POD methodology presented by Meyer (2007). The code uses MATLAB's ability to solve very large eigenvalue problems efficiently. The only requirement for the snapshot POD methodology is that the input data be arranged in a matrix **P** as follows:

$$\boldsymbol{P} = [p^1 p^2 \ldots p^n] = \begin{bmatrix} p_1^1 & \cdots & p_1^n \\ \vdots & \ddots & \vdots \\ p_{16}^1 & \cdots & p_{16}^n \end{bmatrix} \qquad (10)$$

where p^i is the column vector of the 16 pressure data points collected in the simulation and *n* is the number of instantaneous snapshots, i.e. time values in this case.

Analysis of the Pressure Data

In the experiments underway for validation of this analysis 16 wall pressure monitors located 90° apart at downstream locations of 0.4D, 2D, 4D and 6D are used and their location is shown in Fig. 10. Clearly in the CFD many more locations could be used but in any sort of control strategy the number of sampling locations needs to be kept to a minimum.

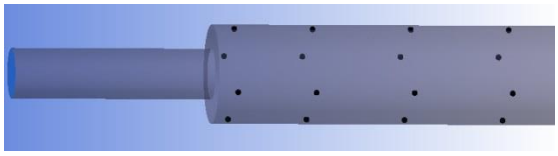

Figure 10: Location of the pressure monitor points in the CFD simulations.

An obvious question related to the use of POD is to determine how long a time period must be sampled to correctly capture the underlying behaviour of the flow. In order to access the transient data, records were truncated to give different sample times and POD was performed on the reduced datasets. Figure 11 shows the cumulative power against number of modes included for sampling times ranging from 1 to 80 s. It is evident that a minimum time of 15 s is required and that the current results that used data for 40 s give decompositions that are independent of the sampling time.

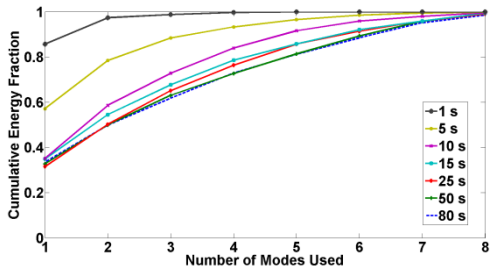

Figure 11: Cumulative power against number of modes as a function of sampling time for Re = 3×10^4 and S = 0.072.

POD analysis for the recorded pressure data over a period of 40 s are given in Figs. 12 and 13 for the *k-ε* run with S = 0.086, Re = 10^5 and the zonal LES case with S = 0.072, Re = 3×10^4, respectively. There are a number of observations that can be made from these figures:

1. As would be expected, the pressure data in Fig. 12(b) are very smooth and regular, compared with those from the zonal LES simulation, shown in Fig. 13(b).
2. In the *k-ε* case only two non-zero modes exist, as shown in Fig. 12(a), compared with 8 in the zonal LES case, as shown in Fig. 13(b). Even in the latter case POD has shown a massive reduction in the amount of data needing to be stored, as only a small number of time-dependent coefficients, a_i, are needed to reproduce the pressure data.
3. In the *k-ε* simulation the first mode captures a large part of one set of pressure traces and the second mode captures the others, so that the sum of the two modes, shown in Fig. 12(d), reproduces the pressure data almost exactly.

4. In the zonal LES case the reconstruction is more complex with the first mode showing a substantial difference (Fig. 13(c)). However, the first 4 modes give a good reconstruction, as seen in Fig. 13(d).

The relationship between the a_i coefficients used to reconstruct the pressure field in eqn. (6) can potentially tell you something about the interaction between the modes (see Liné et al., 2013 for a good description of this reconstruction for flowfields in mixing vessels). Figure 14 shows plots of mode a_1 versus mode a_2 and mode a_1 versus mode a_6 for the two simulations reported in Figs. 12 and 13. It is evident that a regular phase trajectory is established in the pressure data from the *k-ε* simulation but the data are much more chaotic in the zonal LES simulation. Fig. 14(a) shows an elliptical trajectory, indicating that when mode 1 is important mode 2 is unimportant etc. explaining the form of Figs. 12(c) and 12(d). It is clear from these data that whilst there is a strong correlation between the coefficients in the *k-ε* simulation, those from the scale-resolving simulation are much more complex and the phase space plots appear chaotic.

Finally, Fig. 15 shows the accumulated energy as a function of number of modes summed for swirl numbers ranging from 0 to 0.15. It is evident that in all cases around 10-14 modes are sufficient to account for the entire energy of the system. Re = 10^5 in all cases except for S = 0.072 and this case requires fewer modes to achieve an equivalent energy fraction than any other swirling case, possibly because of the lower Reynolds number.

Work is ongoing to extract a physical picture from these data and to collect experimental data for comparison with the CFD results. Snapshot POD is being considered for application to CFD data on a plane to extract the flow structures.

CONCLUSIONS

Simulations of transient flow in an axisymmetric sudden expansion have been conducted using both the *k-ε* and SAS-zonal LES models using ANSYS CFX. It is shown that the *k-ε* model leads to transient behaviour with just two dominant modes, whereas the SAS-zonal LES model captures much more physical behaviour. POD analysis is shown to be very powerful in reducing the size of the transient dataset and has the potential to provide insights into the flow structure and reduced order models for flow control.

ACKNOWLEDGEMENTS

This work was partially funded by ARC Discovery grant DP130103742.

REFERENCES

BIENKIEWICZ, B., TAMURA, Y., HAM, H.J., UEDA, H. and HIBI, K., (1995), "Proper orthogonal decomposition and reconstruction of multi-channel roof pressure", *J. Wind Engng. Ind. Aero.*, **54-55,** 369-381.

BONNET, J.P., COLE, D.R., DELVILLE, J., GLAUSER, M.N. and UKEILEY, L.S., (1994), "Stochastic estimation and proper orthogonal decomposition: complementary techniques for identifying structure", *Exp. in Fluids*, **17,** 307-314.

BORÉE, J., (2003), "Extended proper orthogonal decomposition: A tool to analyse correlated events in turbulent flows", *Exp. in Fluids*, **35,** 188-192.

DELLENBACK, P.S., METZGER, D.E. and NEITZEL, G.P., (1988), "Measurement in turbulent swirling flow through an abrupt axisymmetric expansion", *AIAA J.*, **26**(6), 669-681.

EGOROV, Y., MENTER, F.R. LECHNER, R. and COKLJAT, D, (2010), "The scale-adaptive simulation method for unsteady turbulent flow predictions. Part 2: Application to complex flows", *Flow Turb. Combust.*, **85**, 139-165.

FLETCHER, D.F., GUO, B., HARVIE, D.J.E., LANGRISH, T.A.G., NIJDAM, J.J. and WILLIAMS, J., (2006), "What is important in the simulation of spray dryer performance and how do current CFD models perform?", *Appl. Math. Model.*, **30**(11), 1281-1292.

FLETCHER, D.F. and LANGRISH, T.A.G., (2009), "Scale-adaptive simulation (SAS) modelling of a pilot-scale spray dryer", *Chem. Engng. Res. Des*., **87**(10), 1371-1378.

GUO, B., LANGRISH, T.A.G. and FLETCHER, D. F., (2001), "Simulation of turbulent swirl flow in an axisymmetric sudden expansion", *AIAA J.*, **39**(1), 96-102.

LIANG, Y.C., LEE, H.P., LIM, S.P., LIN, W.Z., LEE, K.H. and WU, C.G., (2002), "Proper orthogonal decomposition and applications – Part 1: theory," *J. Sound Vibration*, **252**, 527-544.

LINE, A., GABELLE, J.-C., MORCHAIN, J., ANNE-ARCHARD, D. and AUGIERE, F., (2013), "On POD analysis of PIV measurements applied to mixing in a stirred vessel with a shear thinning fluid", *Chem. Eng. Res. Des.*, **91**, 2073-2083.

LUMLEY, J., (1967), "The structure of inhomogeneous turbulent flows", In *Atmospheric Turbulence and Radio Wave Propagation*, 166-178, eds. A.M. Yaglom and V.I. Tatarsky, Nuaka, Moscow.

MENTER, F.R., GARBARUK, A., SMIRNOV, P. and COKLJAT, D., (2009), "Scale-adaptive simulation with artificial forcing", Third Symposium on Hybrid RANS-LES Methods, Gdansk, Poland, 10-12 June.

MENTER, F.R. and EGOROV, Y., (2010), "The scale-adaptive simulation method for unsteady turbulent flow predictions. Part 1: Theory and model description", *Flow Turb. Combust*., **85**, 113-138.

MEYER, K.E., PEDERSEN, J.M. and ÖZCAN, O., (2007), "A turbulent jet in crossflow analysed with proper orthogonal decomposition", *J. Fluid. Mech.*, **583,** 199-227.

SIROVICH, L., (1987), "Turbulence and dynamics of coherent structures Part 1: Coherent structures", *Quart. J. Appl. Math.*, **45**, 561-571.

TAYLOR, J.A., and GLAUSER, M.N., (2004), "Toward practical flow sensing and control via POD and LSE based low-dimensional tools", *J. Fluid. Engng.*, **126,** 337-345.

TAMURA, Y. and SUGANUMA, S., (1999), "Proper orthogonal decomposition of random wind pressure field", *J. Fluids and Struct.*, **13,** 1069-1095.

WEGNER, B., STAUFER, M., SADIKI, A. and JANICKA, J., (2007), "Study of flow and mixing in a generic GT combustor using LES", *Flow, Turb. Combust.*, **79**, 389-403.

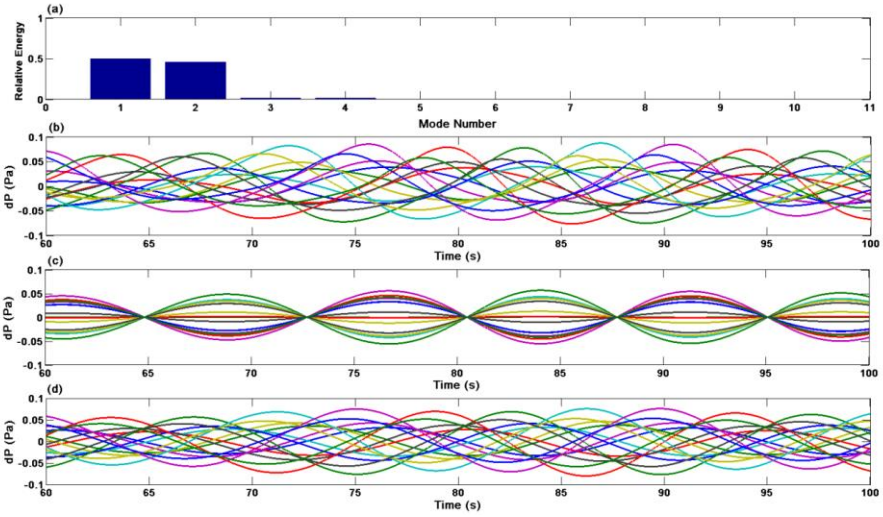

Figure 12: POD analysis of wall pressure data for the *k-ε* simulation with S = 0.086: part (a) shows that only the first two modes are non-zero; part (b) shows the pressure values calculated by CFD over the period 60-100 s; part (c) shows the pressure signal reconstructed using the first eigenvector, and part (d) shows the signal constructed from the first two eigenvectors. The reconstructed pressure traces are indistinguishable from the calculated values.

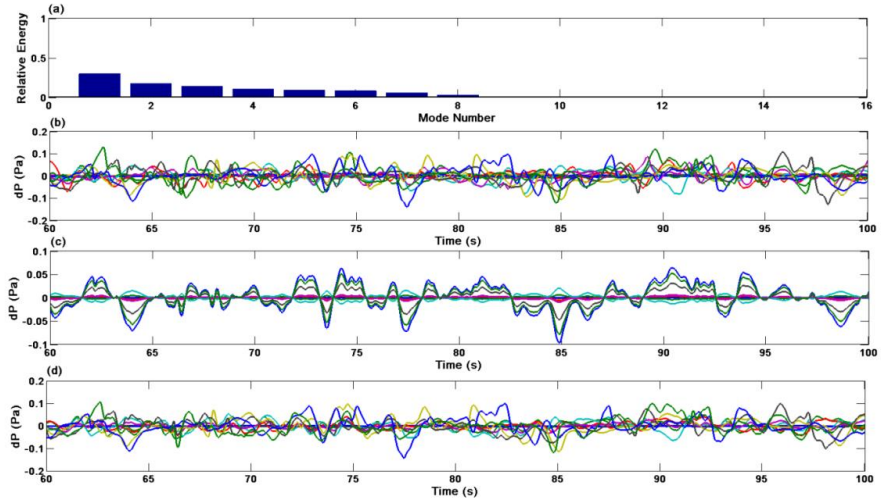

Figure 13: POD analysis of wall pressure data for the zonal LES simulation with S = 0.072, Re = 3×10^4. The layout of the figure is similar to that of Fig. 12 except part (d) shows the sum of the first 4 modes. In this case there are 8 non-zero modes.

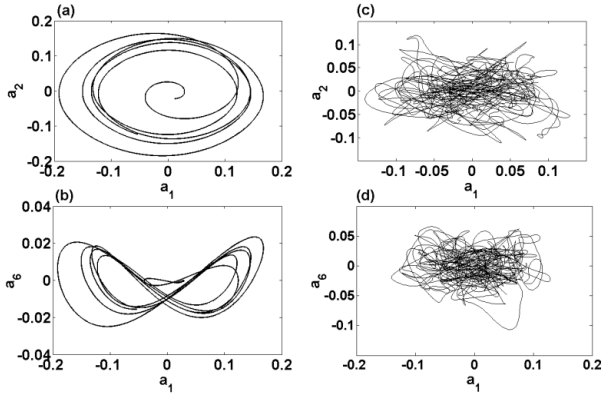

Figure 14: Phase plots showing POD coefficients of mode 1 plotted against mode 2 and mode 1 against mode 6 for results from the k-ε model (a) and (b) and the zonal LES simulation ((c) and (d)) for the data shown in Figs 12 and 13.

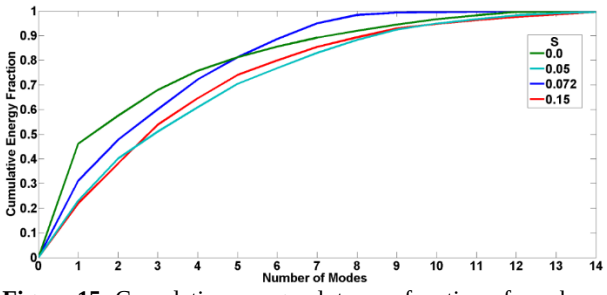

Figure 15: Cumulative energy plots as a function of number of modes for various swirl numbers. Re = 10^5 for all cases except for S = 0.072 where it is 3×10^4.